Theor Chem Acc (2009) 124:319–330
DOI 10.1007/s00214-009-0612-2

REGULAR ARTICLE

Structural and electronic structure differences due to the O–H···O and O–H···S bond formation in selected benzamide derivatives: a first-principles molecular dynamics study

Aneta Jezierska · Jarosław J. Panek · Riccardo Mazzarello

Received: 31 March 2009 / Accepted: 13 July 2009 / Published online: 8 August 2009

Abstract Density functional theory-based methods were employed to obtain static and dynamical descriptions of the molecular properties of 2-hydroxy-*N*-methylbenzamide and 2-hydroxy-*N*-methylthiobenzamide; compounds containing O–H···O and O–H···S strong, intramolecular hydrogen bonds. These compounds are important as analogues of commercial analgesic and antipyretic medicines. In the current study the classical Kohn–Sham method was applied to develop static models describing the geometric parameters and proton potentials. The topological analysis of the electron density was performed via atoms in molecules theory. Subsequently, Car–Parrinello molecular dynamics investigations were performed in vacuo and in the solid state. The geometric and spectroscopic properties were investigated and compared with available experimental data. The influence of quantum effects on the intramolecular hydrogen bond properties were studied via path integral molecular dynamics in the solid state for 2-hydroxy-*N*-methylbenzamide. We found that the proton behavior depends strongly on the type of acceptor: the sulfur-containing bridge has significantly smaller proton flexibility than the oxygen-bearing analogue, which is reflected in the electronic structure and bridge dynamics.

Keywords Intramolecular hydrogen bond · Atoms in molecules · Car–Parrinello molecular dynamics (CPMD) · Path integrals molecular dynamics (PIMD)

1 Introduction

Salicylamides (2-hydroxybenzamide derivatives) are compounds of general interest in medicinal chemistry. The prototypic compound of this series, salicylamide (2-hydroxybenzamide), is a mild analgesic, antipyretic, fungicidal and antirheumatic drug, valuable for its very minor sedative effects [1]. The compound is used industrially as protective antifungal agent in cosmetics [2], and its numerous derivatives have been studied for their stronger analgesic properties at reduced toxicity [3]. Salicylanilides (for example efuamide and niclosamide) are used commercially as antiparasitic, antibacterial, immunosuppressive and anti-inflammatory medicines [4–7]. Close analogues of salicylamides are 2-hydroxythiobenzamides, which were also tested successfully for antibacterial activity [8, 9]. 2-hydroxythiobenzamide is used as ligand for quantitative estimation of Pt(IV) and Au(III) ion concentrations [10–12], while *N*-methylsalicylamide—one of our compounds of interest—is used as a model system for binding of Fe(III) [13]. *N*-methylthiobenzamide was used in a synthetic route to new azapolycyclic compounds based on yohimbane alkaloids [14]. A common feature of various 2-hydroxybenzamides and their thiobenzamide analogues is the presence of intramolecular

Electronic supplementary material The online version of this article (doi:10.1007/s00214-009-0612-2) contains supplementary material, which is available to authorized users.

A. Jezierska
National Institute of Chemistry, Hajdrihova 19, 1001 Ljubljana, Slovenia

Present Address:
A. Jezierska (✉) · J. J. Panek
Faculty of Chemistry, University of Wrocław, 14 F. Joliot-Curie, 50-383 Wrocław, Poland
e-mail: anetka@elrond.chem.uni.wroc.pl

R. Mazzarello
Computational Science, Department of Chemistry and Applied Biosciences, ETH Zurich, USI Campus, via Giuseppe Buffi 13, 6900 Lugano, Switzerland

hydrogen bonds, enabled by close positioning of the 2-hydroxyl as a donor and amide nitrogen atom as a hydrogen bond acceptor.

Recently it has become possible to predict crystal structures on the basis of accurate calculations of intermolecular potentials, with hydrogen bonds constituting key factors determining the crystal packing [15]. Therefore, here we investigate two similar compounds differing only by the choice of the acceptor atom. The chemical and physical effects due to the formation of inter- and intramolecular hydrogen bonds in biologically active systems, as well as in materials science, are intensively discussed issues in the literature [16–18]. Their formation leads to the appearance of various phenomena associated with structural and electronic structure modifications, e.g. in systems containing very short and strong hydrogen bonds proton transfer occurs, which is very important in many processes of biochemistry (e.g. vision, action of enzymatic catalytic triads, electron transfer chains, etc.) [19–21] and in materials science (e.g. rational design of crystalline structures or exploration of solvent- and photo-induced proton transfer) [22–26]. It is worth mentioning that, despite long-lasting experimental and theoretical investigations, the phenomenon of proton transfer is still not fully understood, and there are new theories emerging which are alternatives to the most-accepted "proton transfer coordinate" description of the process [27]. Another very important issue is related to the charge transfer in systems with middle-strong or strong H-bonds. An ultimate example of the importance of charge transfer in the context of hydrogen bonding is the proton-coupled electron transfer, which involves both proton transfer and redox reactions [28]. In the literature one can find many studies where the nature of so-called charge-assisted bonds and the consequences of their formation are discussed [29–33]. Intramolecular hydrogen bridges are usually formed between atoms containing lone electron pairs, especially nitrogen and oxygen, whereas the H-bonds with sulfur atoms as proton acceptors are less known and therefore the nature of this interaction has not been completely elucidated [34, 35]. In the current study, we present ab initio molecular dynamics simulations based on density functional theory (DFT) for two kinds of intramolecular H-bridges and discuss the formation of the H-bond and its influence on the structural and electronic structure parameters. As suitable compounds for the investigations we chose 2-hydroxy-*N*-methylbenzamide and 2-hydroxy-*N*-methylthiobenzamide [36]. These two compounds belong to the family of salicylamides, described above, and their structures and spectroscopic properties are well studied [36, 37]; close analogues [amides, (thio)hydrazides and free (thio)acids] have also been investigated and can serve as reference [38–40]. Furthermore, an additional interesting point is the observation of steric effects of the large sulfur atom on (a) the conformation of the single 2-hydroxy-*N*-methylthiobenzamide molecule, which is twisted, whereas the oxo analogue is planar [36] and (b) the crystal structure packing. More specifically, the two compounds form different crystal motifs (linear chains for the oxo compound, and ziz-zag chains for the thio analogue, in both cases linked via amide-N–H···O-hydroxyl bridges) and networks of intermolecular hydrogen bonds.

This study is an extension of our previous computational investigations of 2-hydroxythiobenzhydrazide and 2-hydroxybenzydrazide [41], where the nature of H-bond bridges was studied in detail using a combination of diverse computational approaches in the gas phase and solid state. The results indicated that the intermolecular contacts were much more localized than intramolecular bridge protons. In the current study, where the -NH-NH_2 moiety of Ref. [41] has been replaced with the -NH-CH_3 group, we shall focus on the properties of the intramolecular hydrogen bonds; however, we would like to point out that in our systems the network formed by the weak intermolecular H-bonds is responsible, together with the van der Waals forces, for the crystal structure stabilization at room temperature [36]. We have investigated previously the proton behavior in some O–H···O and O–H···S bridges, and so far our indications are that the sulfur atom as an acceptor leads to much reduced propensity for proton transfer [34, 41, 42], which is consistent with experimental data [36].

2 Computational methodology

2-hydroxy-*N*-methylbenzamide and 2-hydroxy-*N*-methylthiobenzamide (see Fig. 1) [36] were investigated using DFT [43, 44] and molecular dynamics based on DFT [45, 46] approaches.

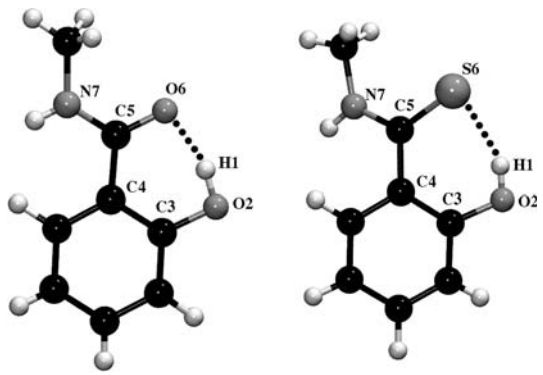

Fig. 1 Structures of studied compounds: 2-hydroxy-*N*-methylbenzamide (*left side*) and 2-hydroxy-*N*-methylthiobenzamide (*right side*). Only atoms of interest are marked

2.1 Static DFT models

This part of the simulations was performed in vacuo to develop static models describing the molecular properties of 2-hydroxy-*N*-methylbenzamide and 2-hydroxy-*N*-methylthiobenzamide [36]. The three-parameter hybrid Becke's functional with correlation energy based on Lee-Yang-Parr formula denoted as B3LYP was used [47, 48]. The double- and triple-zeta split-valence basis sets with diffuse functions on non-hydrogen atoms and polarization functions on all atoms denoted, according to Pople's nomenclature, as 6–31 + G(d,p), 6–311 + G(d,p), 6–31 + G(2d,2p) and 6–311 + G(2d,2p) [49] were employed in the simulations. Harmonic frequencies were calculated to check if the obtained structures correspond to minima of the potential energy surface (PES). Next, the proton potential functions were obtained by placing the hydrogen bridged proton (H1) on a set of points with varying donor–proton distance for the O2–H2···O6 bridge in the case of 2-hydroxy-*N*-methylbenzamide and O2–H1···S6 in the case of 2-hydroxy-*N*-methylthiobenzamide. In these calculations full geometry optimizations were performed, with the exception of the O2–H1 distance, which was constrained as the scanned coordinate. This part of the simulations was performed using the Gaussian03 suite of programs [50], which was additionally used to generate the wave functions for further processing using atoms in molecules (AIM) theory. The description of the electronic structure was prepared in the framework of the AIM theory [51]. The electron density and its Laplacian were evaluated at bond critical points (BCPs) for the studied compounds. Atomic charges according to AIM theory were calculated by numerical integration of the electron density over atomic domains provided by the level of DFT theory. This part of the calculations was performed using the AIMPAC package [52].

2.2 Energy minimization and molecular dynamics according to the Car–Parrinello method

Ab initio molecular dynamics simulations according to the Car–Parrinello method [45] were performed in vacuo and in the solid state. The exchange-correlation functional proposed by J. P. Perdew, K. Burke and M. Ernzerhof (PBE) was employed [53]. Plane-wave basis sets were used, coupled with the norm-conserving pseudopotentials proposed by N. Troullier and J. L. Martins [54] for each type of atom in the studied compounds. The kinetic energy cutoff was set to 100 Ry after performing extensive test calculations to estimate the influence of the cutoff on the geometric parameters of the studied compounds (see Table 2SI). The 100-Ry cutoff was found to be the best value in terms of balance between convergence of structural parameters and computational efficiency. The energy minimization was performed to generate initial conditions for the molecular dynamics runs. The Hessian matrix proposed by Schlegel as an approximation to the exact matrix of second derivatives was used for this purpose [55].

Molecular dynamics simulations in vacuo for 2-hydroxy-*N*-methylbenzamide and 2-hydroxy-*N*-methylthiobenzamide were performed in a cubic cell of $a = 16$ Å with the periodic image removal scheme enabled. The simulations were performed at 298 K and the temperature was controlled by Nosé-Hoover thermostat chains, coupled separately to each degree of freedom [56–58]. The fictitious electron mass μ was set to 400 a.u. A time-step value of 3 a.u. was employed. The initial part of the MD run (ca. 0.75 ps) was used to equilibrate the system and was not taken into account during the analysis of the results. Trajectories with lengths ca. 22 ps were used for the data analysis. Dipole moments were collected as well during the simulations.

Solid-state simulations for 2-hydroxy-*N*-methylbenzamide and 2-hydroxy-*N*-methylthiobenzamide were performed using the structural parameters provided by X-ray experiments (i.e. experimental cell data and atomic coordinates were employed, see Fig. 1SI for the solid-state models) [36]. A few constant volume simulations were also carried out to check the effect of the cell size on the dynamics of the system. In this set of simulations the experimental cell parameters were isotropically scaled by factors varying from 90–110% in 2% increments, and constant volume MD runs were performed at each cell size. Periodic boundary conditions (PBCs) were used in the electrostatic summations, and the Ewald sum was calculated taking into account eight neighbors in each direction. The energy minimizations were performed according to the procedure described above. In addition, convergence with respect to k-points was tested for the experimental unit cell using Γ-point, $2 \times 2 \times 2$, $3 \times 3 \times 3$ and $4 \times 4 \times 4$ Monkhorst-Pack k-point meshes [59]. The geometric parameters of the atoms involved in the intramolecular hydrogen bond obtained by calculations at Γ-point and using $2 \times 2 \times 2$, $3 \times 3 \times 3$ and $4 \times 4 \times 4$ meshes are presented in Table 2SI. They show that the Γ-point approximation is sufficiently good, which is not unexpected, given the rather large simulation cells employed. Therefore, our simulations were performed in the Γ-point approximation using the setup described above. The data, after 0.75 ps of equilibration phase, were collected for ca. 33 ps for 2-hydroxy-*N*-methylbenzamide and 16 ps for 2-hydroxy-*N*-methylthiobenzamide.

Subsequently, the trajectories obtained from the ab initio MD runs in both phases were used:

1. to analyze the time evolution of selected interatomic distances,
2. to calculate the infrared spectra (IR) using atomic velocities and dipole moments. Fourier transformation of the time autocorrelation function of the atomic velocity and dipole moment was performed for this purpose.

2.3 Path integrals molecular dynamics

Path integral molecular dynamics (PIMD) [46, 60, 61] runs were performed in the solid state for both studied compounds. The simulations were carried out at 298 K and controlled by a separate Nosé-Hoover thermostat for each degree of freedom [56–58]. The PIMD simulations were performed with the same settings as described above for the CPMD runs. Eight Trotter replicas were used for the imaginary time path integration. The staging of the path integral propagator was applied during the simulations [61, 62]. The initial part of the simulations (ca. 0.75 ps) was taken as equilibration time and was not further analyzed. The production run consists of ca. 20 ps. Using the PIMD trajectories, a histogram for the analysis of the hydrogen (H1) position in the intramolecular hydrogen bond was prepared.

Car–Parrinello and path integral molecular dynamic simulations were performed using the CPMD program v3.11.1 [63]. The VMD [64] and Gnuplot [65] programs were used for the data graphical presentation.

3 Results and discussion

3.1 Static models on the basis of DFT using various basis sets and plane-waves

Selected calculated geometric parameters are compared to experimental X-ray data [36] in Table 1. The data were obtained from DFT simulations in combination with various localized basis sets, as well as using plane-waves in vacuo and in the solid state within the Car–Parrinello method [45]. All selected bond distances involved in the pseudo-ring formation are reproduced correctly; however, the distances obtained using plane-waves and PBE functionals are slightly shortened in the intramolecular H-bond region compared to the experimental data. The value of the valence

Table 1 Selected experimental (X-ray) and calculated (DFT) interatomic distances (in Å) and O6···H1–O2 and S6···H1–O2 valence angles (in degrees) of 2-hydroxy-*N*-methylbenzamide and 2-hydroxy-*N*-methylthiobenzamide in vacuo (using various localized basis sets and plane waves) and in the solid state (using plane waves)

Interatomic distances	X-ray [36]	B3LYP/ 6-31 + G(d,p)	B3LYP/ 6-311 + G(d,p)	B3LYP/ 6-31 + G(2d,2p)	B3LYP/ 6-311 + G(2d,2p)	CPMD PBE in vacuo	CPMD PBE in the solid state
2-hydroxy-*N*-methylbenzamide							
H1–O2	0.875	0.9961	0.9900	0.9941	0.9908	1.0165	1.0596
O2–C3	1.353	1.3428	1.3411	1.3390	1.3340	1.3423	1.3356
C3–C4	1.395	1.4217	1.4185	1.4195	1.4160	1.4252	1.3808
C4–C5	1.487	1.4866	1.4868	1.4851	1.4847	1.4808	1.4680
C5–O6	1.240	1.2516	1.2435	1.2457	1.2436	1.2589	1.2653
O6···H1	1.666	1.6461	1.6697	1.6414	1.6513	1.5819	1.4586
O6···O2	2.510	2.5499	2.5622	2.5462	2.5510	2.5248	2.4667
C5–N7	1.324	1.3570	1.3562	1.3543	1.3529	1.3583	1.3839
O6···H1–O2 valence angle	161.05	148.64	147.78	149.12	148.80	151.97	156.47
2-hydroxy-*N*-methylthiobenzamide							
H1–O2	0.814	0.9919	0.9875	0.9912	0.9880	1.0180	1.0190
O2–C3	1.359	1.3441	1.3420	1.3395	1.3406	1.3380	1.3501
C3–C4	1.403	1.4245	1.4210	1.4226	1.4191	1.4333	1.4235
C4–C5	1.482	1.4819	1.4810	1.4799	1.4784	1.4727	1.4713
C5–S6	1.679	1.6922	1.6887	1.6889	1.6871	1.7226	1.7292
S6···H1	2.202	2.0731	2.0861	2.0544	2.0661	1.9363	1.9586
S6···O2	2.936	2.9820	2.9895	2.9667	2.9732	2.8938	2.9180
C5–N7	1.323	1.3485	1.3461	1.3456	1.3430	1.3488	1.3327
S6···H1–O2 valence angle	150.25	151.40	151.20	152.08	151.72	155.54	155.79

The data reported for the CPMD were obtained with kinetic energy cutoff = 100 Ry

angle formed by the atoms involved in the intramolecular H-bond is reproduced correctly as well. There is nevertheless an uncertainty in the positions of the hydrogen atoms, especially of those involved in hydrogen bridges, which constitutes a source of discrepancy between the experimental data and the calculated results. Overall, the agreement between experimental and theoretical data is fairly good, given the approximations involved in our DFT calculations. Figures 2SI and 3SI present the energy profiles obtained for the O2–H1 distance changes calculated at four levels of theory in the gas phase. The obtained results show that in both compounds a single energy minimum is present. This fact indicates that, on the basis of static models, the bridged proton prefers to be located at the donor side in the gas phase and proton transfer is disfavored. The amide and thioamide differ significantly in the structure of the intramolecular hydrogen bridge. While the pseudo-ring of the amide is planar (the C3–C4–C5–O6 dihedral angle is 4.4°), it is puckered in the thioamide (the C3–C4–C5–S6 torsion is 27.2°). This fact suggests that the O–H···S bridge is much weaker than its O–H···O analogue. We put every effort to generate structures for the proton-transferred forms of the studied compounds, but we always obtained the molecular forms after energy minimization. The same happened when the solvent reaction field was modeled within the framework of the polarizable continuum model (PCM) solvation technique employing water as a solvent [66].

The last part of this section is devoted to the AIM analysis for both compounds. The application of the AIM theory gave us further insights into the electronic structure differences due to the presence of different atoms in the intramolecular hydrogen bridge. The basic parameters at bond critical points (BCPs), such as the electron density and its Laplacian, and the atomic charges were calculated at various levels of theory for the atoms involved in the pseudo-ring formation (see Table 2 for BCPs parameters and Table 1SI for atomic charges values). The existence of BCPs between O6/S6 and H1 atoms reveals the presence of intramolecular hydrogen bonds in these systems. The positive value of the electron density Laplacian for O6/S6···H1 confirms the dominantly non-covalent character of the hydrogen bonds, whereas the electron density Laplacian values obtained for the H1–O2, O2–C3, C3–C4, C4–C5 and C5–O6/S6 bonds indicate their covalent character (see Table 2). The electron densities and their Laplacians for the O6/S6···H1 contacts agree well with the presence of a strong hydrogen bond and fall within the range of values proposed by Koch and Popelier [67], but the values of the electron density and, especially, its Laplacian decrease when the acceptor atom is sulfur. This fact underlines the weaker character of the O–H···S bond, noticeable already by inspection of the geometrical parameters, as discussed above. The O6···H1 distance is shorter compared to the S6···H1 length in 2-hydroxy-*N*-methylthiobenzamide, which is due to the larger atomic and van der Waals radii of sulfur. A similar conclusion can be drawn for the C5–O6 bond, where the electron density and its Laplacian have higher values with respect to 2-hydroxy-*N*-methylthiobenzamide. The AIM atomic charges analysis indicates large differences between the charge values on O6 and S6 atoms. This can be explained as well from the electron density distribution and the fact

Table 2 Electron density and its Laplacian calculated at bond critical points (BCPs) of the hydrogen bridge of 2-hydroxy-*N*-methylbenzamide and 2-hydroxy-*N*-methylthiobenzamide

Level of theory	2-hydroxy-*N*-methylbenzamide											
	H1–O2		O2–C3		C3–C4		C4–C5		C5–O6		O6···H1	
	ρ	$\nabla^2(\rho)$	ρ	$\nabla^2(\rho)$	ρ	$\nabla^2(\rho)$	ρ	$\nabla^2(\rho)$	ρ	$\nabla^2(\rho)$	ρ	$\nabla^2(\rho)$
B3LYP/6-31 + G(d,p)	0.3276	−1.8791	0.3068	−0.4168	0.3009	−0.7925	0.2699	−0.6750	0.3826	−0.2405	0.0539	0.1530
B3LYP/6-311 + G(d,p)	0.3325	−2.3195	0.3053	−0.4583	0.2980	−.07977	0.2656	−0.6600	0.3878	−0.4451	0.0517	0.1475
B3LYP/6-31 + G(2d,2p)	0.3357	−2.0634	0.3152	−0.7726	0.2988	−0.7166	0.2658	−0.5769	0.3973	−0.5634	0.0551	0.1557
B3LYP/6-311 + G(2d,2p)	0.3382	−2.5131	0.3128	−0.7097	0.3029	−0.8319	0.2665	−0.6465	0.3959	−0.7420	0.0536	0.1421
	2-hydroxy-*N*-methylthiobenzamide											
	H1–O2		O2–C3		C3–C4		C4–C5		C5–S6		S6···H1	
	ρ	$\nabla^2(\rho)$	ρ	$\nabla^2(\rho)$	ρ	$\nabla^2(\rho)$	ρ	$\nabla^2(\rho)$	ρ	$\nabla^2(\rho)$	ρ	$\nabla^2(\rho)$
B3LYP/6-31 + G(d,p)	0.3326	−1.8642	0.3045	−0.3944	0.2983	−0.7784	0.2695	−0.6642	0.2119	−0.1993	0.0389	0.0586
B3LYP/6-311 + G(d,p)	0.3355	−2.2974	0.3035	−0.4398	0.2954	−0.7832	0.2657	−0.6556	0.2135	−0.2710	0.0384	0.0614
B3LYP/6-31 + G(2d,2p)	0.3395	−2.0493	0.3135	−0.7512	0.2959	−0.7014	0.2658	−0.5730	0.2114	−0.3509	0.0419	0.0555
B3LYP/6-311 + G(2d,2p)	0.3416	−2.4975	0.3110	−0.6890	0.2993	−0.8144	0.2673	−0.6489	0.2111	−0.3435	0.0405	0.0557

ρ [ea_0^{-3}] = electron density; $\nabla^2(\rho)$ [ea_0^{-5}] = Laplacian of the electron density

that the interaction between O2–H1···O6 is stronger than that between O2–H1···S6.

3.2 Car–Parrinello molecular dynamics in vacuo and in the solid state

The models used in these simulations are presented in Fig. 1 and Fig. 1SI, respectively. Let us start to discuss our results from the time evolution of the interatomic distances of the atoms involved in the intramolecular hydrogen bond formation. Figure 2 shows data for both compounds obtained by Car–Parrinello molecular dynamics (CPMD) simulations in vacuo. The behavior of hydrogen bonds is similar in both cases. The bridged proton is strongly localized on the donor side and contacts with the acceptor atom are not observed. These results are in agreement with our gas phase static models reported above, in which proton motion along the intramolecular bridge was shown to be restricted. The time evolution of interatomic distances was investigated as well in the solid state for both compounds. The crystal cells contain two molecules and eight molecules in the case of 2-hydroxy-*N*-methylbenzamide and 2-hydroxy-*N*-methylthiobenzamide, respectively. For clarity purposes, from each unit cell only one molecule was selected and its geometric parameters are presented in Fig. 3. The proton transfer phenomenon is present in the case of 2-hydroxy-*N*-methylbenzamide during the simulation time. Additionally, many short contacts are registered as well. The proton is strongly delocalized between the donor and acceptor atoms. An opposite situation is observed in 2-hydroxy-*N*-methylthiobenzamide. The bridged proton is localized on the donor side and even short contacts with the acceptor atoms are absent. Therefore, the crystal field has a strong influence on the molecular properties of 2-hydroxy-*N*-methylbenzamide systems, which contain low barrier hydrogen bonds (LBHBs), whereas in the case of 2-hydroxy-*N*-methylthiobenzamide, the effect of the crystal field appears to be weaker. These conclusions

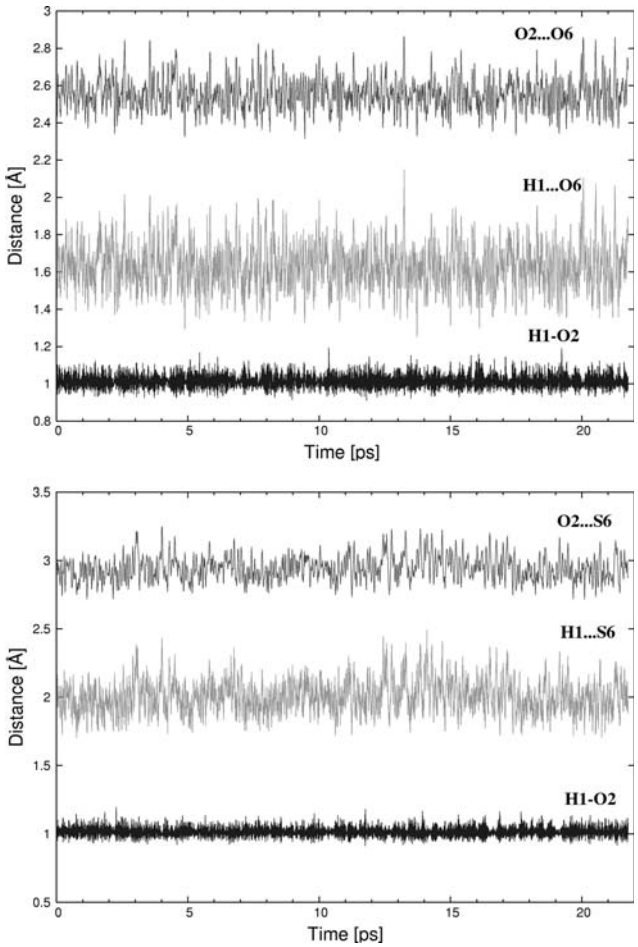

Fig. 2 Time evolution of interatomic distances of atoms involved in intramolecular H-bonds of 2-hydroxy-*N*-methylbenzamide (*upper graph*) and 2-hydroxy-*N*-methylthiobenzamide (*lower graph*); results obtained from Car–Parrinello molecular dynamics in vacuo

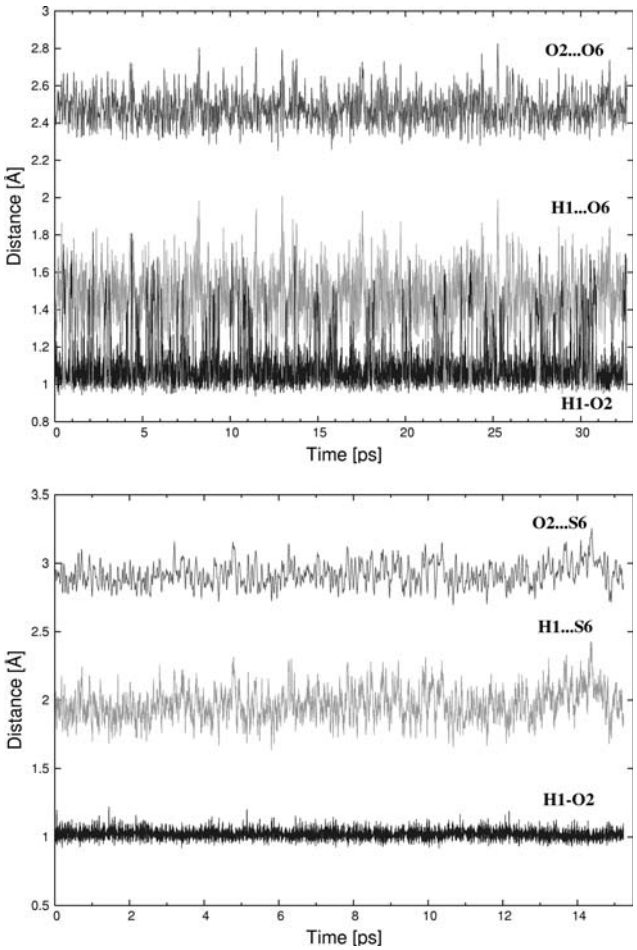

Fig. 3 Time evolution of interatomic distances of atoms involved in intramolecular H-bonds of 2-hydroxy-*N*-methylbenzamide (*upper graph*) and 2-hydroxy-*N*-methylthiobenzamide (*lower graph*); results obtained from Car–Parrinello molecular dynamics in the solid state

are in agreement with our previous investigations of analogous compounds in the solid phase [41, 42]. We should stress that the internal crystal field might be smaller than the average field due to the presence of a liquid polar environment (e.g. water as a solvent); however, the crystal field is highly ordered and anisotropic, in contrast to the latter, and can thus have a more dramatic effect on the properties of hydrogen bonds. The anisotropy of the local environment around the hydrogen bridges is different for the two studied crystals; the benzamide derivative forms linear chains in the crystal phase, while its thio analogue forms zig-zag motifs [36]. This fact, together with the differences in the chemical properties of sulfur and oxygen, is responsible for the contrasting behavior of the hydrogen bond in the two systems. The obtained results correspond well with numerous studies on the behavior of sulfur as proton acceptor [68–71]. The sulfur atom is considered as a soft base in terms of Pearson's hard-soft acid-base (HSAB) concept, and as such is less reactive towards very hard acids, such as an acidic proton. This fact was also proven by interaction energy decomposition calculations [68], which indicated ca. two times larger contribution of dispersion forces for O–H···S in comparison with corresponding O–H···O systems. Additionally, H and S have similar electronegativities, in contrast to H and O, which results in reduced proton-accepting abilities for the sulfur atom [69]. Experimental matrix isolation studies of H_2O_2 complexes with various bases [70] have shown that the O–H···S bond is weaker energetically than the O–H···O bond in corresponding systems; these findings are in agreement with recent supersonic jets experiments as well [68]. However, it is possible to induce proton transfer and tautomerism in some aromatic systems with intermolecular O–H···S bond [71]. There is one additional factor which might affect the proton behavior: since sulfur has a relatively low electronegativity as discussed above (Pauling scale: 2.58, compared to 3.44 for O, 2.20 for H and 2.55 for C [72]), the C = S group is less polar than the carbonyl moiety, which might upset the stabilizing "resonance" effect due to the formation of the proton-transferred form [32, 33].

We have also tested the influence of unit cell size on the properties of 2-hydroxy-*N*-methylbenzamide, as mentioned in Sect. 2. The results obtained are presented in Fig. 4SI. The decrease of the cell volume led to a sharp increase of the internal stress tensor, while the simulations with cell axes enlarged more than a factor of 1.04 led systematically to negative values of the stress tensor. Remarkably, the model obtained by a 104% enlargement of the cell axes (Fig. 4SI) also displays frequent short-lived proton transfers to the acceptor: however, the transitions are less abundant than in the model with the experimental cell parameters. This fact also suggests that the electrostatic crystal field should be a major factor responsible for the behavior of the intramolecular bridge of the studied benzamide.

To further clarify these points, we calculated the correlation histograms for the O2–H1 and O2···O(S)6 distances. A comparison of these histograms for in vacuo and solid-state simulations for both 2-hydroxy-*N*-methylbenzamide and -thiobenzamide is presented in Fig. 4. The presence of neighboring molecules has rather minor effects on the dynamical structural behavior of the O2···S6 intramolecular bridge. On the other hand, proton sharing is greatly increased for the O2···O6 bridge in the solid state, in accordance with the time evolution of the bridge parameters (Fig. 3). The upper histogram shows that the proton is still located dominantly at the donor side, but at reduced bridge lengths there is a high probability of temporary proton transfer to the acceptor atom.

The spectroscopic properties of the studied compounds were investigated on the basis of dipole moments and atomic velocity power spectra. Experimental data [37]

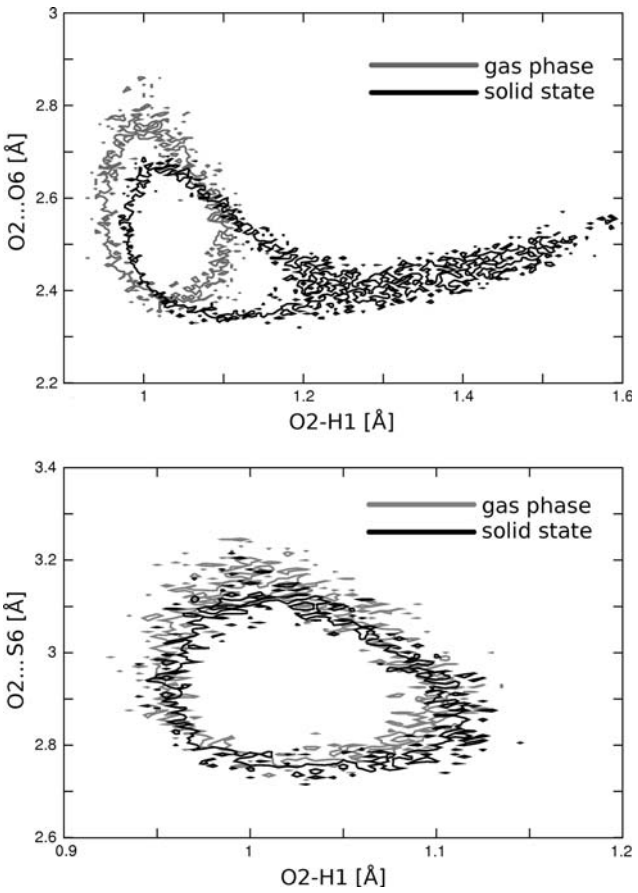

Fig. 4 Correlation histogram of the O2–H1 and O2–O6 distances for 2-hydroxy-*N*-methylbenzamide (*upper graph*) and O2–H1 and O2–S6 distances for 2-hydroxy-*N*-methylthiobenzamide (*lower graph*) obtained from Car–Parrinello molecular dynamics in vacuo and in the solid state. Probability density isocontours at 5 $Å^{-2}$

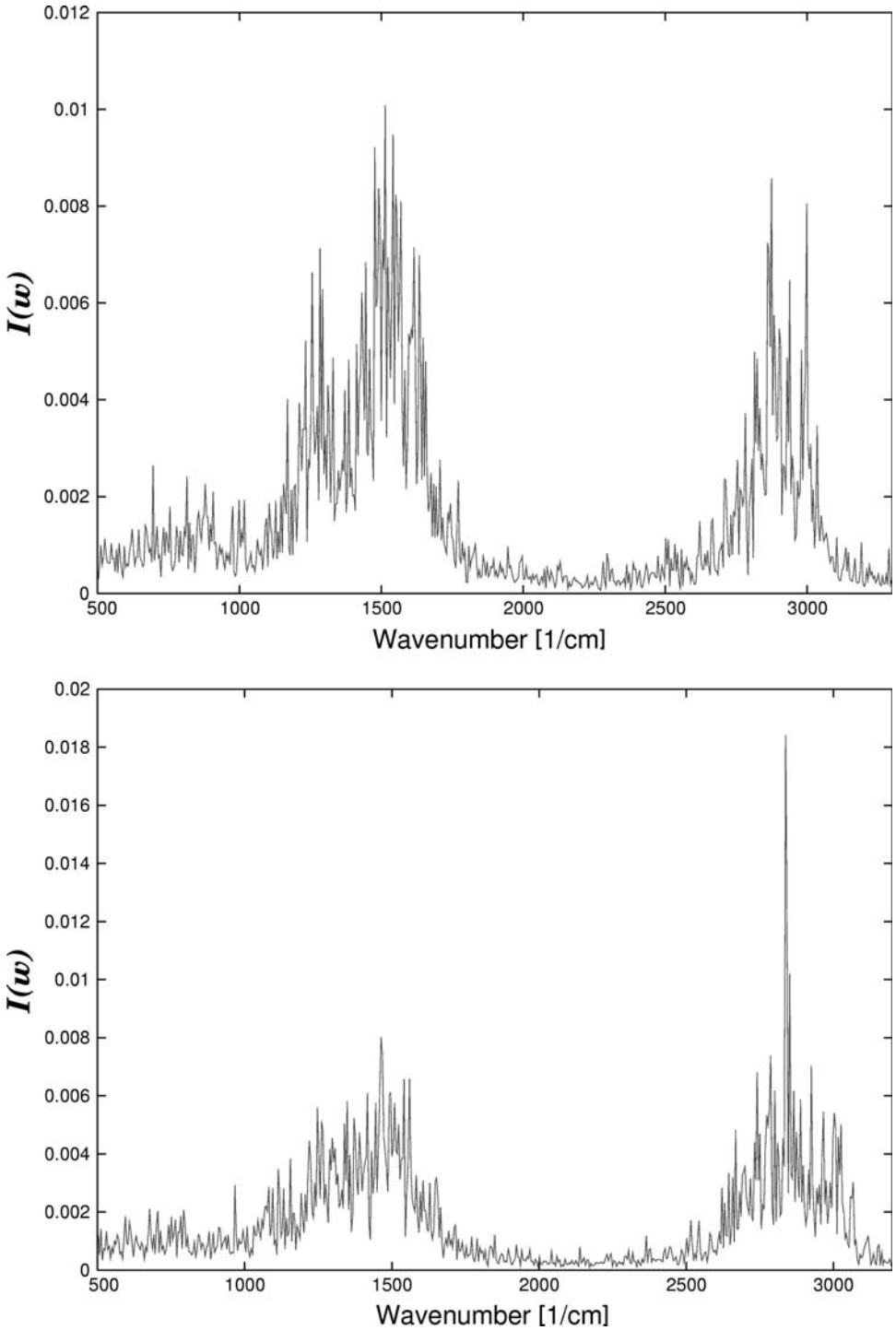

Fig. 5 IR spectra of 2-hydroxy-*N*-methylbenzamide (*upper graph*) and 2-hydroxy-*N*-methylthiobenzamide (*lower graph*) calculated from Car–Parrinello molecular dynamics in vacuo

report that the studied (thio)amides have relatively broad absorptions caused by the intramolecular O–H···O(S) bridges, while the amide N–H bond modes are quite sharp (see Fig. 5SI for a redrawing of the original experimental data). The O–H(···O) stretching band of 2-hydroxy-*N*-methylbenzamide is centered at ca. 2950 cm^{-1} in CCl_4, which is red-shifted to 2700 cm^{-1} in the solid state (fluorolube mull). Corresponding data for 2-hydroxy-*N*-methylthiobenzamide are: 3000 cm^{-1} in CCl_4, and 2840 cm^{-1} in the fluorolube mull. The N–H bands are located between 3319 and 3484 cm^{-1}. Interestingly, the solution ^1H NMR shifts of the O–H protons (12.16 ppm for the amide and 11.13 ppm for the thioamide) confirm that the thio-bridge is weaker, and these shifts are larger than those of the N–H protons (6.15 and 7.60 ppm, respectively) [37]. The experimental IR and NMR data on the

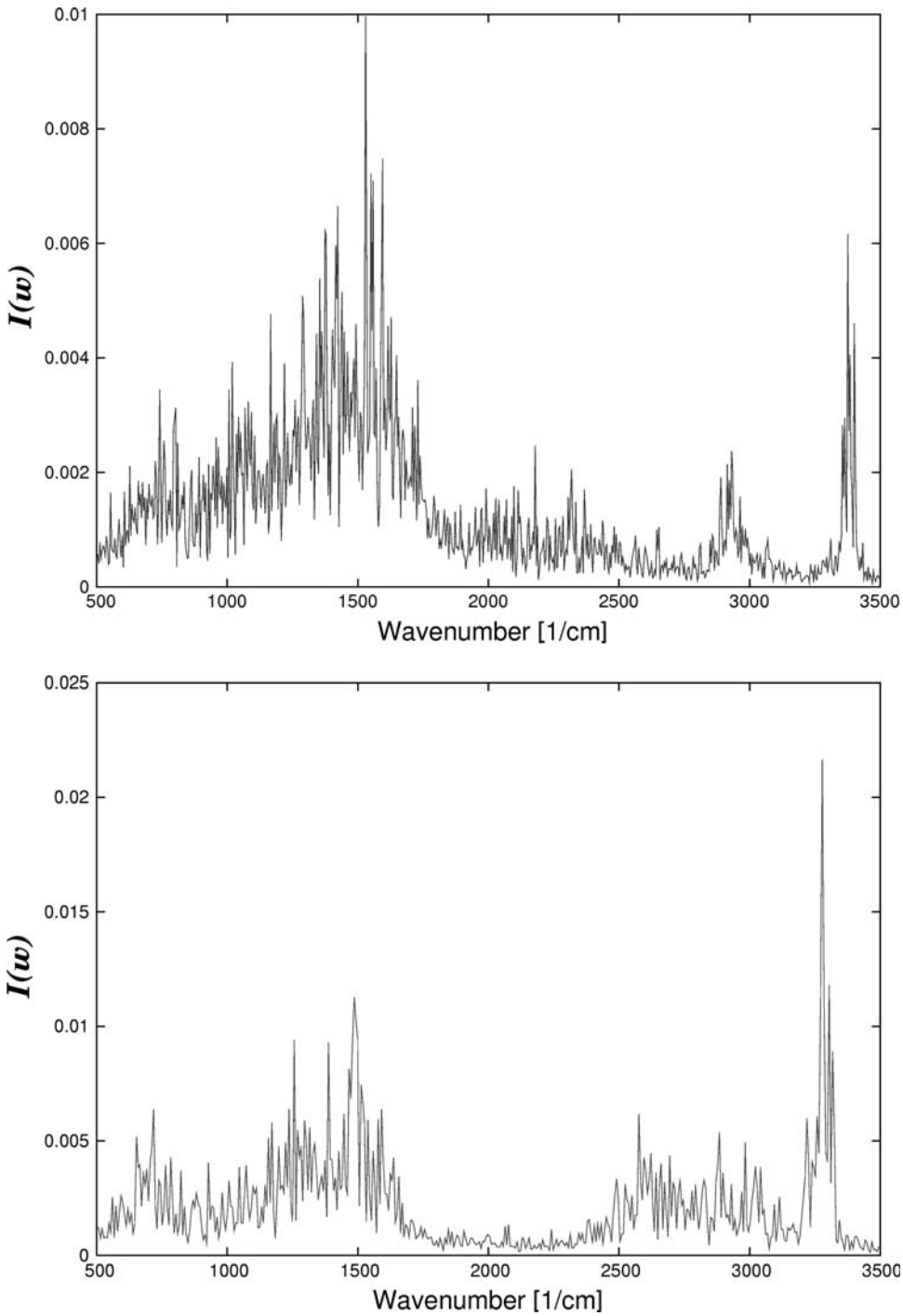

Fig. 6 IR spectra of 2-hydroxy-*N*-methylbenzamide (*upper graph*) and 2-hydroxy-*N*-methylthiobenzamide (*lower graph*) calculated from Car–Parrinello molecular dynamics in the solid state

intramolecular bridge properties compare well to those yielded by our CPMD simulations. First, gas-phase IR spectra (Fig. 5) show that both amide and thioamide have broad absorptions located in the 2600–3200 cm^{-1} region, centered at 2800–2900 cm^{-1} (the small red shift in comparison to the experiments is a combined effect of the approximated DFT functional used and the CPMD method, which introduces a "drag effect" to the nuclear motion [73–75]). The situation changes when the spectrum is calculated in the solid state (Fig. 6). The amide with its delocalized proton exhibits broad absorption (in good agreement with the experimental spectrum, cf. Fig. 5SI of this work and Fig. 1 of Ref. [37]), while the thioamide bridge signal is diffuse, but restricted to the 2500–3000 cm^{-1} region. These results were confirmed by isolation of the contributions of the intramolecular bridge protons to the total motion intensity (Fig. 7), which allows for the identification of the O–H stretching regions.

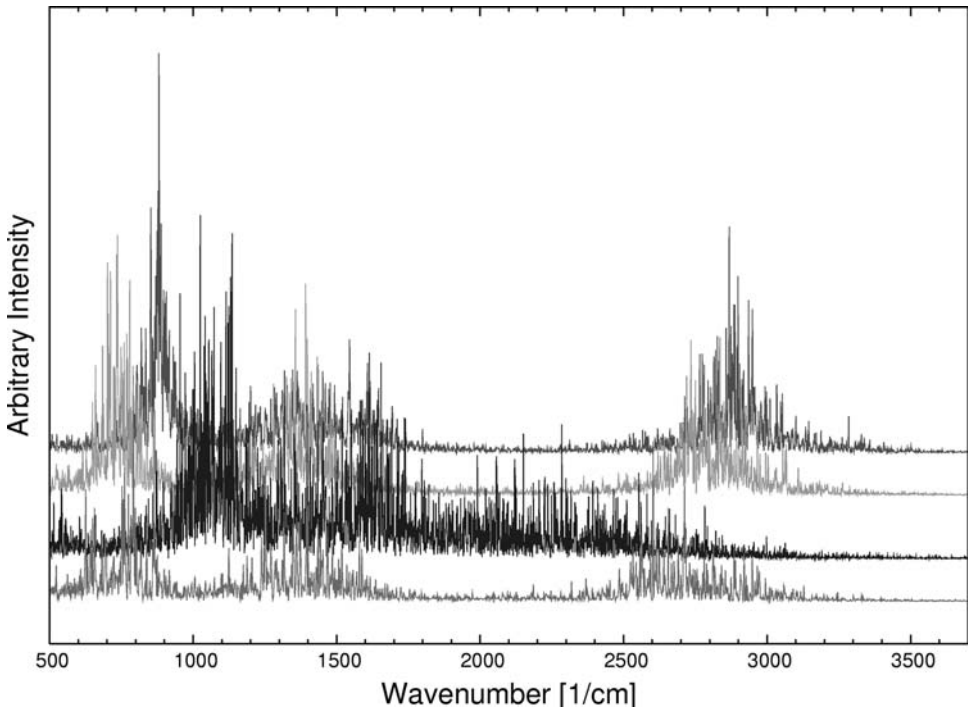

Fig. 7 Power spectra of bridged protons in 2-hydroxy-*N*-methylbenzamide and 2-hydroxy-*N*-methylthiobenzamide respectively, obtained from Car–Parrinello molecular dynamics in vacuo (*two upper curves*) and in the solid state (*two lower curves*)

3.3 Path integral molecular dynamics in the solid state

The inclusion of quantum effects in the description of the motion of protons and light atoms favors their delocalization by two mechanisms: exploration of larger portions of the phase space due to the delocalization of the nuclear wave function, and tunneling [76]. PIMD simulations were performed for 2-hydroxy-*N*-methylbenzamide only, since it was recently shown that quantum effects do not play an important role in compounds similar to 2-hydroxy-*N*-methylthiobenzamide [34]. Figure 8 shows how the results of the PIMD for 2-hydroxy-*N*-methylbenzamide compare to the calculations obtained within the classical approximation for nuclei. Proton delocalization is increased and the O2–H1 coordinate of the isocontour barycenter is shifted from 1.08 Å to the value of 1.15 Å. This elongation of the donor–proton distance is accompanied by a decrease in the total bridge length. Additionally, the delocalization of the proton has partially masked the correlation between the O2–H1 and O2···O6 structural parameters. It is not possible to provide time-resolved information on the quantum effects, e.g. mean time between tunneling events or proton jumps, because the PIMD formulation recovers only statistically averaged information on the quantum ensemble.

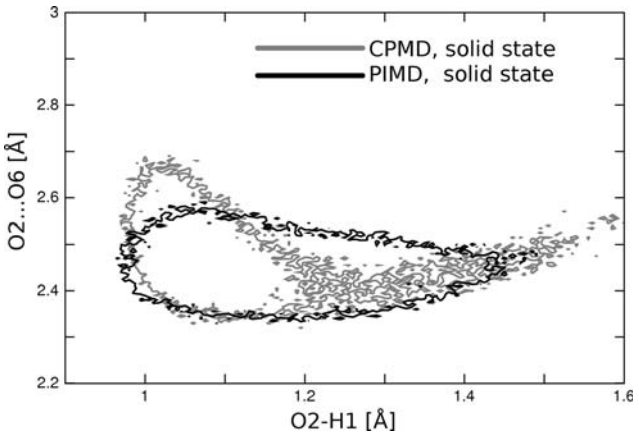

Fig. 8 Correlation histogram of the O2–H1 and O2–O6 distances for 2-hydroxy-*N*-methylbenzamide calculated from Car–Parrinello and path integral molecular dynamics simulations in the solid state. Probability density isocontours at 5 $Å^{-2}$

4 Conclusions

We have shown that the use of combined static and dynamical approaches to the description of the molecular properties of 2-hydroxy-*N*-methyl(thio)benzamide successfully reproduces experimental data and provides insight into the nature of the two analogous intramolecular hydrogen bridges. In particular, we have found that:

- in agreement with experiments, the O–H···S bond is weaker than the O–H···O analogue, revealing the decreased ability of sulfur as proton acceptor: this fact is due to the chemical differences between oxygen and sulfur, in particular to the smaller electronegativity difference between sulfur and hydrogen atoms in comparison with the H···O case. These conclusions

are supported by the calculated structural parameters and electronic structure (AIM data) in static models in vacuo and the results of extensive ab initio molecular dynamics simulations;

- in the solid-state calculations, the interplay between crystal field effects and the above mentioned differences in the chemical properties of S and O has a strong impact on the details of proton dynamics in the bridge; both its time-resolved structural data and spectroscopic signatures. As a result, the probability of proton transfer in 2-hydroxy-*N*-methylbenzamide is strongly enhanced as compared to 2-hydroxy-*N*-methylthiobenzamide.

Acknowledgments We would like to thank Dr. Harald Forbert (Ruhr-Universität Bochum) for the program for dipole moment transformations. We also gratefully acknowledge the Academic Computer Center (TASK) in Gdańsk and the Poznań Supercomputing and Networking Center (PCSS) for providing CPU time and facilities.

References

1. Soldatos CR, Kales A, Bixler EO, Scharf MB, Kales JD (1978) Pharmacol 16:193–198
2. Kirk RE, Othmer DF (1997) Kirk-Othmer encyclopedia of chemical technology, vol 21, 4th edn. Wiley, New York, pp 601–626
3. Way EL, Takemori AE, Smith GE Jr, Anderson HH, Brodie DC (1953) J Pharmacol Exp Ther 108:450–460
4. Fuente De La R, Sonawane ND, Arumainayagam D, Verkman AS (2006) Br J Pharmacol 149:551–559
5. Zhu X-F, Wang J-S, Cai L-L, Zeng Y-X, Yang D (2006) Cancer Sci 97:84–89
6. Agrawal VK, Sharma S (1984) Pharmazie 39:373–378
7. Brown ME, Fitzner JN, Stevens T, Chin W, Wright CD, Boyce JP (2008) Bioorg Med Chem 16:8760–8764
8. Wagner G, Singer D, Weuffen W (1966) Pharmazie 21:161–166
9. Weuffen W, Wagner G, Singer D, Hellmuth L (1966) Pharmazie 21:477–482
10. Sur K, Shome SC (1971) Anal Chim Acta 57:201–208
11. Sur K, Mazumdar M, Shome SC (1972) Anal Chim Acta 59:306–310
12. Banerjee K, Raychaudhury S (1982) Bull Chem Soc Jpn 55:3621–3624
13. Hay BP, Dixon DA, Vargas R, Garza J, Raymond KN (2001) Inorg Chem 40:3922–3935
14. Padwa A, Beall LS, Heidelbaugh TM, Liu B, Sheehan SM (2000) J Org Chem 65:2684–2695
15. Price SL (2009) Acc Chem Res 42:117–126
16. Jeffrey GA (1997) An introduction to hydrogen bonding. Oxford University Press, New York
17. Grabowski S (2006) Hydrogen bonding—new insights. Challenges and advances in computational chemistry and physics 3. Springer, Dordrecht
18. Hobza P, Havlas Z (2000) Chem Rev 100:4253
19. Saam J, Tajkhorshid E, Hayashi S, Schulten K (2002) Biophys J 83:3097–3112
20. Haas AH, Lancaster CRD (2004) Biophys J 87:4298–4315
21. Betzel C, Gourinath S, Kumar P, Kaur P, Perbandt M, Eschenburg S, Singh TP (2001) Biochemistry 40:3080–3088
22. Bertolasi V, Gilli P, Ferretti V, Gilli G (1996) Chem Eur J 2:925–934
23. Tour JM, Kozaki M, Seminario JM (1998) J Am Chem Soc 120:8486–8493
24. Alarcón SH, Olivieri AC, Sanz D, Claramunt RM, Elguero J (2004) J Mol Struct 705:1–9
25. Sobczyk L, Grabowski SJ, Krygowski TM (2005) Chem Rev 105:3513–3560
26. Hammes-Schiffer S (2001) Acc Chem Res 34:273–281
27. Peters KS (2009) Acc Chem Res 42:89–96
28. Iordanova N, Hammes-Schiffer S (2002) J Am Chem Soc 124:4848–4856
29. Szatyłowicz H, Krygowski TM, Hobza P (2007) J Phys Chem A 111:170–175
30. Szatyłowicz H, Krygowski TM, Zachara-Horeglad JE (2007) J Chem Inf Model 47:875–886
31. Szatyłowicz H (2008) J Phys Org Chem 21:897–914
32. Gilli G, Bellucci F, Ferretti V, Bertolasi V (1989) J Am Chem Soc 111:1023–1028
33. Gilli P, Bertolasi V, Ferretti V, Gilli G (1994) J Am Chem Soc 116:909–915
34. Jezierska A, Panek JJ (2009) J Comput Chem 30:1241–1250
35. Steiner T (1998) Chem Commun 411–412
36. Pertlik F (1992) Z Kristallogr 202:17–23
37. Steinwender E, Mikenda W (1990) Monatsh Chem 121:809–820
38. Mikenda W, Pertlik F, Steinwender E (1993) Monatsh Chem 124:867–875
39. Mikenda W, Steinwender E, Mereiter K (1995) Monatsh Chem 126:495–504
40. Pertlik F (1990) Monatsh Chem 121:129–139
41. Jezierska A, Novič M, Panek JJ (2009) Pol J Chem 83:799–819
42. Jezierska A, Panek JJ, Koll A (2008) Chem Phys Chem 9:839–846
43. Hohenberg P, Kohn W (1964) Phys Rev 136:B864–B871
44. Kohn W, Sham LJ (1965) Phys Rev 140:A1133–A1138
45. Car R, Parrinello M (1985) Phys Rev Lett 55:2471–2474
46. Marx D, Parrinello M (1996) Science 271:179–181
47. Becke AD (1993) J Chem Phys 98:5648–5652
48. Lee C, Yang W, Parr RG (1988) Phys Rev B 37:785–789
49. Krishnan R, Binkley JS, Seeger R, Pople JA (1980) J Chem Phys 72:650–654
50. Frisch MJ, Trucks GW, Schlegel HB, Scuseria GE, Robb MA, Cheeseman JR, Montgomery JA Jr, Vreven T, Kudin KN, Burant JC, Millam JM, Iyengar SS, Tomasi J, Barone V, Mennucci B, Cossi M, Scalmani G, Rega N, Petersson GA, Nakatsuji H, Hada M, Ehara M, Toyota K, Fukuda R, Hasegawa J, Ishida M, Nakajima T, Honda Y, Kitao O, Nakai H, Klene M, Li X, Knox JE, Hratchian HP, Cross JB, Bakken V, Adamo C, Jaramillo J, Gomperts R, Stratmann RE, Yazyev O, Austin AJ, Cammi R, Pomelli C, Ochterski JW, Ayala PY, Morokuma K, Voth GA, Salvador P, Dannenberg JJ, Zakrzewski VG, Dapprich S, Daniels AD, Strain MC, Farkas O, Malick DK, Rabuck AD, Raghavachari K, Foresman JB, Ortiz JV, Cui Q, Baboul AG, Clifford S, Cioslowski J, Stefanov BB, Liu G, Liashenko A, Piskorz P, Komaromi I, Martin RL, Fox DJ, Keith T, Al-Laham MA, Peng CY, Nanayakkara A, Challacombe M, Gill PMW, Johnson B, Chen W, Wong MW, Gonzalez C, Pople JA (2004) Gaussian 03, revision C.02. Gaussian Inc., Wallingford, CT
51. Bader RFW (1990) Atoms in molecules. A quantum theory. Clarendon Press, Oxford
52. Bader RFW (1991) AIMPAC, suite of programs for the theory of atoms in molecules. McMaster University, Hamilton, ON
53. Perdew JP, Burke K, Ernzerhof M (1996) Phys Rev Lett 77:3865–3868
54. Troullier N, Martins JL (1991) Phys Rev B 43:1993–2006
55. Schlegel HB (1984) Theor Chim Acta 66:333–340

56. Nosé S (1984) Mol Phys 52:255–268
57. Nosé S (1984) J Chem Phys 81:511–519
58. Hoover WG (1985) Phys Rev A 31:1695–1697
59. Monkhorst HJ, Pack JD (1976) Phys Rev B 13:5188–5192
60. Marx D, Parrinello M (1996) J Chem Phys 104:4077–4082
61. Tuckerman ME, Marx D, Klein ML, Parrinello M (1996) J Chem Phys 104:5579–5588
62. Tuckerman ME, Berne BJ, Martyna GJ, Klein ML (1993) J Chem Phys 99:2796–2808
63. CPMD Copyright IBM Corp. 1990–2004, Copyright MPI fuer Festkoerperforschung Stuttgart 1997–2001
64. Humphrey W, Dalke A, Schulten K (1996) J Mol Graph 14:33–38
65. Gnuplot, Copyright (C) 1986–1993, 1998, 2004 Williams T, Kelley C, Copyright (C) 2004–2007 Broeker HB, Campbell J, Cunningham R, Denholm D, Elber G, Fearick R, Grammes C, Hart L, Hecking L, Koenig T, Kotz D, Kubaitis E, Lang R, Lehmann A, Mai A, Steger C, Tkacik T, Van der Woude J, Van Zandt JR, Woo A, Merritt E, Mikulík P, Zellner J
66. Mennucci B, Tomasi J (1997) J Chem Phys 106:5151–5158
67. Koch U, Popelier PLA (1995) J Phys Chem 99:9747–9754
68. Biswal HS, Chakraborty S, Wategaonkar S (2008) J Chem Phys 129:184311
69. Desiraju GR (2002) Acc Chem Res 35:565–573
70. Goebel JR, Ault BS, Del Bene JE (2001) J Phys Chem A 105:11365–11370
71. Posokhov Y, Gorski A, Spanget-Larsen J, Duus F, Hansen PE, Waluk J (2001) Chem Phys Lett 350:502–508
72. Pauling LJ (1932) J Am Chem Soc 54:3570–3582
73. Tangney P, Scandolo S (2002) J Chem Phys 116:14–24
74. Wathelet V, Champagne B, Mosley DH, André J-M, Massidda S (1997) Chem Phys Lett 275:506–512
75. Gaigeot M-P, Sprik M (2003) J Phys Chem B 107:10344–10358
76. Benoit M, Marx D (2005) Chem Phys Chem 6:1738–1741